The Astrophysical Journal, 654:L5–L8, 2007 January 1

NEW MEASUREMENTS OF COSMIC INFRARED BACKGROUND FLUCTUATIONS FROM EARLY EPOCHS

A. Kashlinsky,[1,2] R. G. Arendt,[1,2] J. Mather,[1] and S. H. Moseley[1]

Received 2006 September 18; accepted 2006 October 30; published 2006 December 22

ABSTRACT

Cosmic infrared background fluctuations may contain a measurable contribution from objects inaccessible to current telescopic studies, such as the first stars and other luminous objects in the first gigayear of the universe's evolution. In an attempt to uncover this contribution, we have analyzed the GOODS data obtained with the *Spitzer* Infrared Array Camera (IRAC). These data are deeper and cover larger scales than the *Spitzer* data that we have previously analyzed. Here we report these new measurements of the cosmic infrared background fluctuations remaining after removing cosmic sources to fainter levels than before. The remaining anisotropies on scales ~0.5′–10′ have a significant clustering component with a low shot-noise contribution. We show that these fluctuations cannot be accounted for by instrumental effects or by the solar system and Galactic foreground emissions and that they must arise from extragalactic sources.

Subject headings: cosmology: observations — diffuse radiation — early universe

1. INTRODUCTION

The cosmic infrared background (CIB) contains emissions from all luminous objects, including those inaccessible to current telescopic studies (see Kashlinsky 2005 for recent review). If the first stars (commonly called Population III) were massive (Abell 2002; Bromm et al. 1999; Bromm & Larson 2004), they could produce significant levels of the CIB with measurable fluctuations (Santos et al. 2002; Salvaterra & Ferrara 2003; Kashlinsky et al. 2004; Cooray et al. 2004; Madau & Silk 2005; Fernandez & Komatsu 2006). Recently, in an attempt to uncover these signatures of early stars, we have detected significant CIB fluctuations after removing galaxies to faint limits in deep *Spitzer* data (Kashlinsky et al. 2005, hereafter KAMM). The measured fluctuations cannot arise from the solar system and Galactic foreground emissions or from the remaining galaxies, and therefore they must come from early extragalactic sources, particularly the first stars. To solidify these findings, we have now analyzed deeper data sets from the Great Observatories Origins Deep Survey (GOODS; Dickinson et al. 2003) covering different and larger areas of the sky and with observing procedures that allow us to test for a wide range of systematic errors in the data.

In this Letter we present the new measurements using the GOODS *Spitzer*/IRAC data at 3.6, 4.5, 5.8, and 8 μm. At the magnitude limit of the QSO 1700 data (from QSO HS 1700+6416), we measure a similar CIB signal consistent with its cosmological origin. After removing still fainter sources, we find that the bulk of the CIB fluctuations remain out to ~10′, the limit of our fields. This shows that the signal originates in populations significantly fainter than our cutoff. We also test for possible systematic errors in the fluctuations by cross-correlating the data for the same regions taken at different epochs and in different detector orientations, showing only a small contribution from the instrument systematics. The Galactic and zodiacal foregrounds are also generally small, although as in the QSO 1700 data, we find the possibility of significant cirrus pollution of the channel 4 fluctuations. Cosmological interpretation of the results is given in a companion paper (Kashlinsky et al. 2007).

2. DATA PROCESSING

Table 1 shows the parameters of the data used in this and earlier (KAMM) analyses. The new data from the GOODS *Spitzer* Legacy Program[3] (Dickinson et al. 2003) come from measurements in two parts of the sky, the Hubble Deep Field–North (HDF-N) and the Chandra Deep Field–South (CDF-S), observed at two different epochs, E1 and E2, ~6 months apart. The two epochs had different detector orientations rotated by ~180° with respect to the sky, allowing us to test for certain instrumental effects and zodiacal light. The final mosaics were assembled from the individual Basic Calibrated Data frames that were self-calibrated using the method of Fixsen et al. (2000), similarly to processing in KAMM; no extended source calibration factors were applied to the data. To evaluate the random noise level of the maps, alternate calibrated frames for each data set were mapped into separate "A" and "B" mosaics.

The assembled maps were cleaned of resolved sources in two steps: First, an iterative procedure was applied that computed the standard deviation, σ, of the image and masked pixels exceeding $N_{\rm cut}\sigma$ (along with $N_{\rm mask} \times N_{\rm mask}$), surrounding the pixels until none exceeded $N_{\rm cut}\sigma$. We adopted $N_{\rm mask} = 3$ and $N_{\rm cut} = 4$, when enough pixels (≥65%) remained for robust Fourier analysis. Second, similar to KAMM, we subtracted the model of the individual sources using a variant of the CLEAN algorithm (Högbom 1974). In a normal CLEAN procedure, the clean components are convolved with an idealized clean beam to produce a map without sidelobe artifacts; we stop short of this, working with the residual map from which the dirty beam and its artifacts have been removed. We construct the model from the original unmasked mosaics for each channel as follows: (1) the maximum pixel intensity is located, (2) the point-spread function is then scaled to half of this intensity and subtracted from the image, and (3) the process is iterated, saving the intermediate results.

Because spectroscopic redshifts are unavailable and resolving individual sources is difficult in the confusion limit of these observations, we removed the sources via the model to a fixed level of the shot noise. Its amplitude due to remaining sources

[1] Observational Cosmology Laboratory, Code 665, NASA Goddard Space Flight Center, Greenbelt MD 20771; kashlinsky@milkway.gsfc.nasa.gov.
[2] Science Systems and Applications, Inc. (SSAI), 10210 Greenbelt Road, Suite 600, Lanham, MD 20706.

[3] PID 194, pipeline ver. S11.4.0, except S11.0.2 for CDF-S E1.

TABLE 1
ANALYZED FIELDS

PARAMETER	QSO 1700	HDF-N		CDF-S	
		E1	E2	E1	E2
(l_{Gal}, b_{Gal}) (deg)	(94.4, 36.1)	(125.9, 54.8)	(125.9, 54.8)	(223.6, −54.4)	(223.6, −54.4)
$(\lambda_{E\,cl}, \beta_{E\,cl})$ (deg)	(194.3, 83.5)	(148.4, 57.3)	(148.4, 57.3)	(41.1, −45.2)	(41.1, −45.2)
Size (arcmin)	5.1 × 11.5	10.2 × 10.2	10.2 × 10.2	8.8 × 8.4[a]	9.0 × 8.4[b]
$\langle t_{obs}\rangle$ (hr)[c]	7.8	20.9	20.7	23.7	22.4
Channel 1 (3.6 μm)					
P_{SN} (nW^2 m^{-4} sr^{-1})	5.8×10^{-11}	1.9×10^{-11}	1.9×10^{-11}	2.2×10^{-11}	2.3×10^{-11}
Zodiacal flux (nW m^{-2} sr^{-1})	32	45–47	37–38	48–51	48–49
Cirrus flux (nW m^{-2} sr^{-1})	2.5	0.8	0.8	0.8	0.8
Channel 2 (4.5 μm)					
P_{SN} (nW^2 m^{-4} sr^{-1})	6.0×10^{-11}	1.1×10^{-11}	1.0×10^{-11}	9.5×10^{-12}	1.1×10^{-11}
Zodiacal flux (nW m^{-2} sr^{-1})	132	174–185	146–153	189–204	165–176
Cirrus flux (nW m^{-2} sr^{-1})	2.7	1.3	1.3	1	1
Channel 3 (5.8 μm)					
P_{SN} (nW^2 m^{-4} sr^{-1})	6.0×10^{-10}	1.2×10^{-10}	1.3×10^{-10}	1.5×10^{-10}	1.5×10^{-10}
Zodiacal flux (nW m^{-2} sr^{-1})	873	1192–1250	996–1026	1256–1327	1179–1243
Cirrus flux (nW m^{-2} sr^{-1})	7.8	3.6	3.6	2.6	2.6
Channel 4 (8 μm)					
P_{SN} (nW^2 m^{-4} sr^{-1})	4.4×10^{-10}	1.0×10^{-10}	1.1×10^{-10}	1.1×10^{-10}	1.4×10^{-10}
Zodiacal flux (nW m^{-2} sr^{-1})	1723	2411–2500	2012–2054	2509–2614	2454–2562
Cirrus flux (nW m^{-2} sr^{-1})	33.8	16.1	16.1	10.1	10.1

[a] 9.′0 × 8.′4 for channels 2 and 4.
[b] 8.′8 × 8.′4 for channels 2 and 4.
[c] For channel 1. Other channels may vary by as much as 0.5 hr, except for the QSO 1700 region where $\langle t_{obs}\rangle = 9.2$ hr.

is $P_{SN} = \int_{m_{lim}}^{\infty} [S(m)]^2 (dN/dm) dm$. $S(m)$ is the flux of magnitude m in units of nW m^{-2}; diffuse flux is defined as νI_ν, with I_ν being the surface brightness in units of MJy sr^{-1}. With the model iteration, in which the maps remain close to a fixed P_{SN}, we can probe the CIB fluctuations produced by populations below a relatively well-defined flux threshold. In principle, the remaining instrument noise, truncated of its high *positive* peaks, may have an imprint of the beam and may mimic part (or even most) of the shot noise from cosmic sources. In that case, the shot noise that we present in Figure 1 represents an *upper* limit on the contribution from cosmic sources, making our conclusions below stronger.

The maps, clipped and with the model subtracted, were Fourier-transformed and subjected to all of the same tests as in KAMM; the additional tests that are possible with this data are described below. The fluctuation field, $\delta F(\boldsymbol{x})$, was not weighted for the results presented here (although we checked that weighting by the observation time in each pixel does not lead to any appreciable changes), and its Fourier transform, $f(\boldsymbol{q}) = \int \delta F(\boldsymbol{x}) \exp(-i\boldsymbol{x}\cdot\boldsymbol{q}) d^2x$, was calculated using the fast Fourier transform. The two-dimensional power spectrum is defined as $P_2(q) \equiv \langle |f_q|^2 \rangle$, and in this definition a typical flux fluctuation is $\simeq [q^2 P_2(q)/2\pi]^{1/2}$ on the angular scale of wavelength $2\pi/q$. The blanked pixels were assigned $\delta F = 0$, thereby not adding power to the eventual power spectrum. Muxbleed was removed by zeroing the corresponding frequencies in the (u, v)-plane before computing the power spectrum of the maps, P_S. We subtracted the remaining linear gradients from the maps before clipping and again after clipping. The noise power spectrum, P_N, was evaluated from the $\frac{1}{2}(A - B)$ data using the mask from the main maps. The remaining power spectrum was evaluated as $P = P_S - P_N$.

3. RESULTS

Figure 1 shows results from the new data compared to the earlier QSO 1700 data analysis. As discussed above, in the present analysis, we can regulate the faint source removal from the maps by fixing the floor level of the shot noise, whose amplitude P_{SN} was evaluated from the fits to the small-scale power spectrum using our model for the beam. Because we mapped the GOODS data onto 1.″2 pixels (instead of onto 0.″6 pixels as for the QSO 1700 data), the beam used for generating the model was a slightly smoothed version of that used in the QSO 1700 data.

The upper panels in Figure 1 show the CIB fluctuations in the GOODS fields evaluated at the model iteration when P_{SN} roughly corresponds to that in the earlier QSO 1700 analysis. The figure shows CIB fluctuations consistent with those in the earlier analyzed QSO 1700 data set. Our results consistently show that at the same level of P_{SN}, all data are probing the same populations (at the deeper model iterations, extra galaxy populations were removed in the present analysis compared to the QSO 1700 field, and at shallower model iterations, extra galaxy populations were removed in the QSO 1700 field). Because of the longer integration in the new data, we can remove sources to still lower P_{SN}. The lower panels of Figure 1 show the CIB fluctuations remaining in the maps at the lowest common value of P_{SN}; the signal shown here comes from still fainter sources than the limits in the earlier KAMM analysis.

4. DISCUSSION

The following can, in principle, contribute to the detected fluctuations: (1) instrumental (systematic and random) effects, (2) source artefacts, (3) solar system and Galactic foregrounds, and (4) extragalactic sources. We briefly discuss the contributions of each and conclude that (with the possible exception

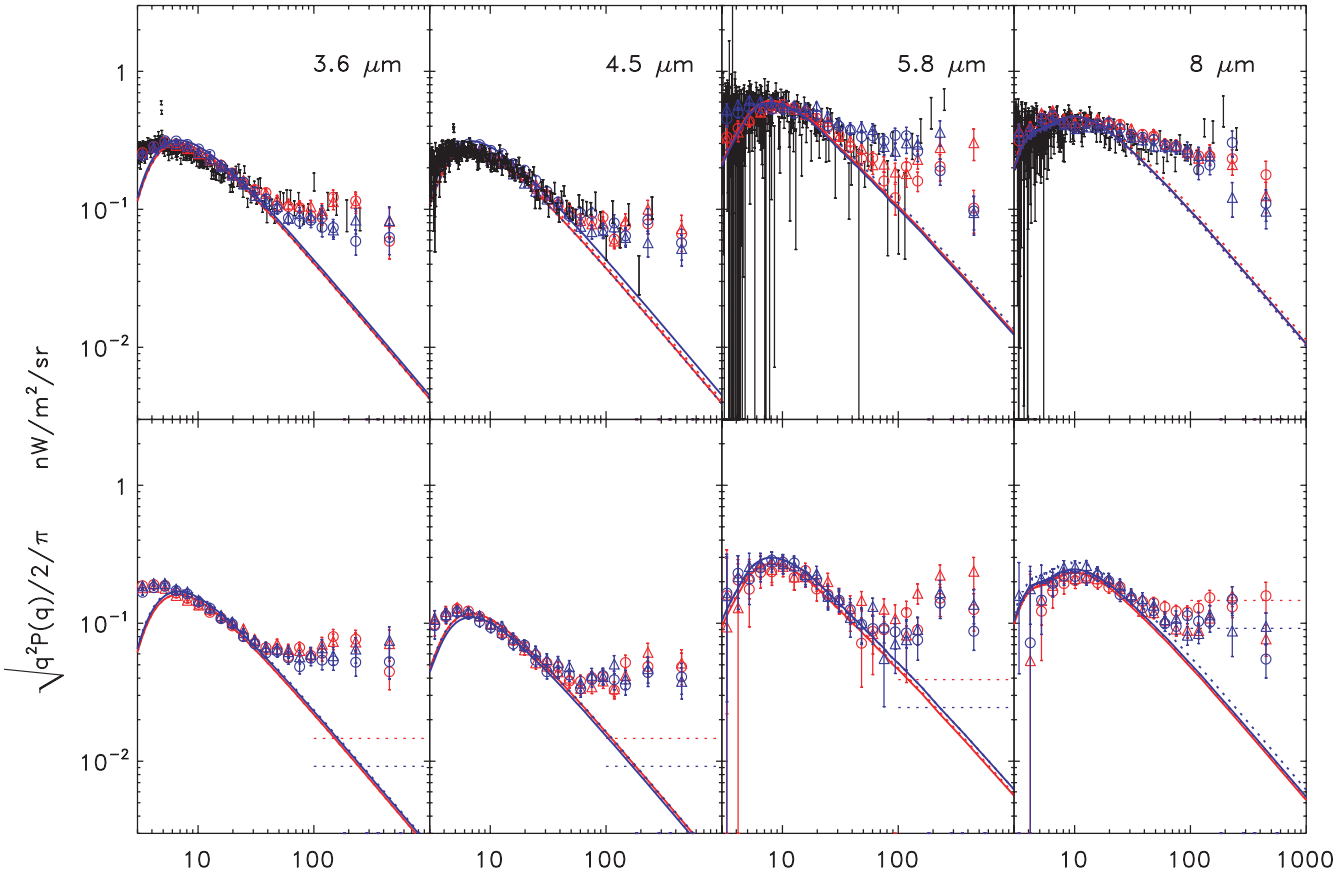

FIG. 1.—CIB fluctuations from the analyzed fields. The fluctuation spectrum was evaluated by averaging over the center of the concentric rings at a given q, and the errors shown correspond to the cosmic variance for the estimates, i.e., the Poissonian errors of relative amplitude $N_q^{-1/2}$, with N_q being the number of independent Fourier elements used in determining the power at q. *Top panels*: CIB fluctuations were evaluated for the shot-noise levels approximately corresponding to the P_{SN} of the QSO 1700 data. The black error bars show the QSO 1700 field results from KAMM. The red symbols correspond to the HDF-N fields, and blue symbols denote the CDF-S data results. Triangles correspond to E1, and circles to E2. The lines show the fluctuations due to shot noise from the remaining sources. *Bottom panels*: Same as the top panel, but shown for the lowest levels of P_{SN} reached with the new data. The blue and red dotted horizontal lines show the estimated cirrus fluctuations for the CDF-S and HDF-N fields, respectively.

of the 8 μm data) the detected fluctuations are due to CIB from extragalactic sources below our removal threshold set by the shot-noise amplitude.

Checking for systematics: E1 versus E2.—In measuring the faint, low spatial frequency backgrounds, control of systematic errors remains a major challenge. Of particular concern is scattered light in the *Spitzer* IRAC optical systems, which can spread the light from point sources over large spatial scales. Some scattered light retains a fixed relative position with respect to the originating point source. Other scattered light gets to the focal plane after multiple reflections, and its spacing with respect to the originating source will vary as the source is moved in the field of view. Finally, some scattered light may arise from sources outside the field of view and may change its illumination of the detector in a complex way as the telescope is moved on the sky. Given that scattered light and detector artifacts can cause structure in the image, it is important that we use observations for these studies that allow us to evaluate the size of such possible effects in the images we analyze.

To search for instrumental sources of large-scale power, we used the partially overlapping E1 and E2 data of the HDF-N and CDF-S regions in which the telescope and optical system are rotated by ~180° with respect to the field of view. Using such observations, we can compare the source-removed sky maps from the two epochs in order to separate structure that is unchanged in inertial coordinates, and thus presumably arising from the sky, from structure that changes, which could represent an instrumental contribution.

We selected overlapping subfields for the final mosaicked images that had fairly homogeneous exposures. The latter limited the selected areas to approximately the same size: 142″ × 504″ in the CDF-S and 149″ × 504″ in the HDF-N. We then computed the subfield and cross-subfield correlation functions and coefficients to verify that the signal is the same at each epoch and is independent of detector orientation. Having carried out the point-source subtraction and gradient removal on the two epochs, we compared the correlation function of the difference map to that of each of the individual maps, and we also did a cross-correlation analysis. In both cases, we find that all of the large-scale power arises from the sky down to the presented statistical error bars; this rules out any significant contribution from instrumental scattered light and detector artifacts.

We also estimated that there is at most only a small contribution to the measured power spectrum from image artefacts, such as those, e.g., associated with occasional strong muxbleed. This was done by selecting subregions, excluding the areas of obvious artefacts (which is responsible for the slight excess in power at 3.6 μm around 1′–2′ for one of the fields).

Procedural sources of large-scale power.—Because IRAC's calibration does not include zero-flux closed-shutter data, a

degeneracy remains in the absolute zero point of the solution. A similar degeneracy is present with respect to first-order gradients in the mosaics. However, higher order gradients are not degenerate. Because of these degeneracies, linear gradients have been fitted and subtracted from the self-calibrated mosaicked images. The zero level is unimportant to this study, so all analyzed maps are set to a mean intensity equal to zero.

We find—via simulations—that in a small but nonnegligible number of cases, the gradient subtraction can also remove the genuine cosmic power at the largest scales and that the power shown there should thus be treated as the *lower* limit on any cosmic fluctuations. However, we find that in the QSO 1700, HDF-N E1, and HDF-N E2 analyses, the results do not change appreciably even if the extra subtraction is done at *each* step of the model iteration. The CDF-S fields, which have a common overlap at both epochs, exhibit more sensitivity (at the level of ~20% in the largest bins) to this extra gradient subtraction. Taken together, this is consistent with the cosmic nature of the fluctuations shown in Figure 1 and with the CDF-S fields happening to be statistically more sensitive to the extra gradient subtraction.

The possible contributions from incompletely removed galaxies are also small, as discussed in KAMM. In brief, (1) the measured fluctuations are independent of the masking and clipping parameters. For example, when clipping is $N_{\rm cut} = 2$, only 6% of the maps remained (KAMM), but the correlation function, which replaces the power spectrum as a measure of large-scale correlations for such deeply cut maps, remained practically the same. (2) The results are invariant when the masking size around each clipped pixel is increased (from $N_{\rm mask} = 3$ to 7). This mask is larger than the typical galaxy size at $z \gtrsim 0.1$, so individual galaxies are expected to have been removed completely. The model further removes much of the remaining emissions at larger angles. (3) We measure the clustering component from ~0.′5 to ~5′–10′, which subtends 1–10 Mpc at $z = 0.1$–1. If the power comes from the incompletely removed local galaxies, its angular spectrum should reflect the slope of the observed galaxy two-point correlation function, contrary to Figure 1. (4) The results are the same for all fields at the fixed level of shot noise. The level of the remaining $P_{\rm SN}$ fixes the amount of the remaining flux from incompletely removed sources of full magnitude *m*. The contribution from them to the large-scale clustering should then have been a proportional fraction of the CIB clustering produced by the parental sources. (5) By the construction in their results, KAMM identified the appropriate model iteration number where the clean components become largely uncorrelated with the sources in the original image (here we use $P_{\rm SN}$ as the alternative criterion).

Zodiacal and Galactic foregrounds.—The cirrus fluxes in Table 1 are the SPOT (*Spitzer* Planning and Observation Tool) estimates of interstellar medium (ISM) intensity, based on the Schlegel et al. (1998) 100 μm *IRAS* intensity and temperature maps and a spectral scaling relation derived from the *Cosmic Background Explorer* (*COBE*) Diffuse Infrared Background Experiment (DIRBE), the *Infrared Space Observatory*, and AROME observations of the ISM (Reach & Boulanger 1997).[4] Fluctuations in the cirrus emission are assumed to be at the 1% level, as suggested by the intensity of the fluctuation spectrum of a low Galactic latitude field in which cirrus emission was clearly evident at 8 μm (KAMM). As in the QSO 1700 data, the cirrus may contribute a nonnegligible contribution at 8 μm and prevents us from isolating the cosmological signal there. Even assuming that the entire signal at 8 μm is produced by cirrus, taking the mean Galactic cirrus energy distribution (Arendt et al. 1998) gives an upper limit on the cirrus emission at shorter wavelengths well below the signal we detect.

The range in zodiacal light intensity in the time spanned by the observations is shown in Table 1. Its fluctuations are a factor of ≃4–15 below those from cirrus. A limit of $\delta F < 0.1$ nW m^{-2} sr^{-1} at 8 μm due to zodiacal light was derived by KAMM from the observed dispersion of the data at two epochs separated by about 6 months. This limit at 8 μm (with relative fluctuations at a much lower level than the <0.2% limit by Ábrahám et al. 1997 at 25 μm) was then scaled to the shorter wavelengths using the zodiacal light spectrum derived from *COBE*/DIRBE data (Kelsall et al. 1998). In the present study too, we find no evidence of zodiacal emission above the instrument noise levels; the arcminute limits on zodiacal fluctuations from subtracting the two epochs are $\delta F \lesssim 0.05$ nW m^{-2} sr^{-1} at 8 μm.

Extragalactic sources.—The detected signal is thus due to CIB fluctuations from extragalactic sources, such as ordinary galaxies and the putative Population III. KAMM estimated that the CIB flux from the remaining galaxies was only ≃0.15 nW m^{-2} sr^{-1}, so that they were unlikely to account for the strong clustering signal. The present data enable us to eliminate intervening sources down to lower levels of the shot noise, or lower flux limits. The detected signal has to originate in still fainter sources. In a companion paper (Kashlinsky et al. 2007), we discuss the constraints our results (both the shot noise and the clustering components of the fluctuations) place on the nature of the sources contributing them. We show that the signal at 3.6–4.5 μm must arise from very faint populations with individual fluxes ≲10–20 nJy and that the amplitude of the fluctuations at arcminute scales requires these populations to be significantly more luminous per unit mass than the present-day ones.

This work is supported by NSF grant AST-0406587 and by NASA *Spitzer* grant NM0710076.

[4] See http://ssc.spitzer.caltech.edu/documents/background/bgdoc_release.html.

REFERENCES

Abell, T. 2002, Science, 295, 93
Ábrahám, P., Leinert, Ch., & Lemke, D. 1997, A&A, 328, 702
Arendt, R. G., et al. 1998, ApJ, 508, 74
Bromm, V., Coppi, P. S., & Larson, R. B. 1999, ApJ, 527, L5
Bromm, V., & Larson, R. 2004, ARA&A, 42, 79
Cooray, A., Bock, J. J., Keatin, B., Lange, A. E., & Matsumoto, T. 2004, ApJ, 606, 611
Dickinson, M., et al. 2003, in The Mass of Galaxies at Low and High Redshift, ed. R. Bender & A. Renzini (New York: Springer), 324
Fernandez, E. R., & Komatsu, E. 2006, ApJ, 646, 703
Fixsen, D. J., Moseley, S. H., & Arendt, R. G. 2000, ApJS, 128, 651
Högbom, J. A. 1974, A&AS, 15, 417
Kashlinsky, A. 2005, Phys. Rep., 409, 361
Kashlinsky, A., Arendt, R., Gardner, J. P., Mather, J. C., & Moseley, S. H. 2004, ApJ, 608, 1
Kashlinsky, A., Arendt, R. G., Mather, J., & Moseley, S. H. 2005, Nature, 438, 45 (KAMM)
———. 2007, ApJ, 654, L1
Kelsall, T., et al. 1998, ApJ, 508, 44
Madau, P., & Silk, J. 2005, MNRAS, 359, L37
Reach, W. T., & Boulanger, F. 1997, in Infrared Emission from Interstellar Dust in the Local Interstellar Medium: The Local Bubble and Beyond, ed. D. Breitschwerdt, M. J. Freyburg, & J. Trümper (Berlin: Springer), 352
Salvaterra, R., & Ferrara, A. 2003, MNRAS, 339, 973
Santos, M. R., Bromm, V., & Kamionkowski, M. 2002, MNRAS, 336, 1082
Schlegel, D. J., Finkbeiner, D. P., & Davis, M. 1998, ApJ, 500, 525